

# Flow patterns in a fluid-saturated porous cube heated from below

By I. SEZAI

Department of Mechanical Engineering, Eastern Mediterranean University, Magosa, Mersin 10, Turkey

(Received 21 October 2003 and in revised form 22 July 2004)

Natural convection in a cube of fluid-saturated porous medium heated from below and cooled from the top is studied numerically using a non-Darcy flow model. All vertical sidewalls are considered to be impermeable and adiabatic. The evolution of the various flow patterns is investigated from onset up to a Rayleigh number of 1000 where irregularly fluctuating convection prevails. New flow patterns have been found to exist in addition to those mentioned in the previous studies. In the present study, a total of ten steady flow patterns have been identified, of which five show oscillatory behaviour in some Rayleigh-number range. The results are presented in terms of average Nusselt number curves consisting of the solution branches of the convective patterns. The convective patterns are classified in terms of their symmetry properties, and the symmetries broken or gained during bifurcations from one flow structure to the other are identified.

---

## 1. Introduction

Convective flow in porous media has been investigated extensively owing to its relevance to practical problems encountered in industrial applications and geological systems. There are numerous studies on the evolution of the convective patterns from stationary state to steady flow and then to unsteady chaotic regime in a two-dimensional porous cavity heated from below. The studies of Horne & O'Sullivan (1974), Caltagirone (1975), Kimura, Schubert & Straus (1987), Riley & Winters (1991), Schubert & Straus (1982), Graham & Steen (1994) are just a few examples of two-dimensional work on a fluid-saturated porous cavity heated from below and cooled from the top, with adiabatic sidewalls. On the other hand, studies on three-dimensional thermal convection in porous media are limited.

According to linear theory, convection begins in a cube of porous medium heated from below and cooled at the top, with insulated vertical sides, when the Rayleigh number  $Ra^*$  equals  $4\pi^2$  (Beck 1972). This is the value obtained by Lapwood (1948) for a horizontally unbounded fluid layer in a porous medium heated from below. In a cubic box, a single-roll two-dimensional flow pattern forms when convection first starts. A three-dimensional flow pattern, having two diagonal rolls, forms for  $Ra^* > 4.5\pi^2$ . This pattern was referred to as the (1, 1, 1) mode (Kimura, Schubert & Straus 1989) as it involves coupled disturbances in all three orthogonal directions. Steen (1983) has shown that the (1, 1, 1) mode is unstable in the range  $4.5\pi^2 \leq Ra^* \leq 4.87\pi^2$ . In addition to the two-dimensional roll cell structure, in the slightly supercritical regime, Zebib & Kassoy (1978) found a coexisting three-dimensional flow pattern, which is formed by the superposition of two horizontal orthogonal two-dimensional rolls.

One of the earliest attempts to investigate the three-dimensional convection in a fluid-saturated porous cube was given by Holst & Aziz (1972) for  $Ra^* = 60$  and 120

using the finite-difference solution of the governing equations. They found that both two- and three-dimensional convection patterns can coexist. This is verified by Horne (1979), who used finite differences up to  $Ra^* = 400$ , and by Straus & Schubert (1979), who used a Galerkin technique to study steady convection in a cube for  $Ra^* = 150$  and later extended the calculations for Rayleigh numbers up to 500 (Schubert & Straus 1979). By means of an analytic eigenfunction-expansion technique, Steen (1983) obtained the regions within the space of the initial conditions which lead to one or other of the competing states and, thereby, the probability that a certain pattern will be realized.

Using a numerical scheme based on the pseudo-spectral method, Kimura *et al.* (1989) determined that the so-called (1, 1, 1) mode becomes oscillatory at a Rayleigh number of 575. Graham & Steen (1991) set this value at  $Ra^* = 584$ . Both studies report that the flow pattern becomes less symmetric prior to the onset of time dependence. Stamps, Arpaci & Clark (1990) found that regularly fluctuating convection begins at  $Ra^*$  between 550 and 560 from steady three-dimensional flow.

It should be noted that all the above studies are based on the Darcy law assumption where the convection terms in the momentum equations are neglected. In these studies, slip boundary conditions were used, which admit no shear stress at the solid walls. This is valid in low-permeability porous media where the strong viscous dissipation through the fluid eliminates the effects of inertia and the formation of a viscous boundary layer. In that case, the slip boundary conditions (no shear) at the walls become the appropriate boundary conditions. When the permeability of the porous medium is high, the drag effect due to the solid matrix and the effect of viscous stresses near the solid walls may become important. For this reason, non-Darcy effects have been included in the present model, where the drag effect is accounted for by including the Forcheimer term. The effect of the wall shear stresses is included through the use of the Brinkman term and no-slip boundary conditions are used at the solid walls. Even though the contribution of the advection terms is small in porous media, they are included in the model to handle all possible situations. At low  $Ra^*$  values, the results of the present model generally agree with previous results found under the assumption of Darcy law and zero shear stress at the solid boundaries. However, for  $Ra^* > 130$ , new flow patterns have been found to exist in addition to those mentioned in the previous studies. In the present study, a total of ten steady-flow patterns have been identified of which five show oscillatory behaviour in some Rayleigh-number range. However, the oscillatory convection of only the (1, 1, 1) pattern has been identified in all previous studies of three-dimensional convection in a porous cube. In the present study, the (1, 1, 1) mode, hereinafter referred to as S3, shows no oscillatory behaviour. At  $Ra^* = 610$ , it bifurcates either into a steady symmetric two-roll pattern, or into a non-symmetric oscillatory pattern.

In the present study, the existence of multiple flow patterns in a fluid-saturated porous cube heated from below and cooled from the top with insulated sidewalls, has been investigated numerically using a non-Darcy model and no-slip boundary conditions. The branches of solutions and bifurcations between the branches, have been shown in a Nusselt number versus Rayleigh number diagram.

## 2. Mathematical formulation

All results are obtained for a fluid-saturated porous medium contained in a cube ( $L_x = L_y = L_z = 1$ ) heated from below and cooled from the top with insulated vertical sides (figure 1). The bottom wall is at a uniform temperature  $T_h$ , while the top wall

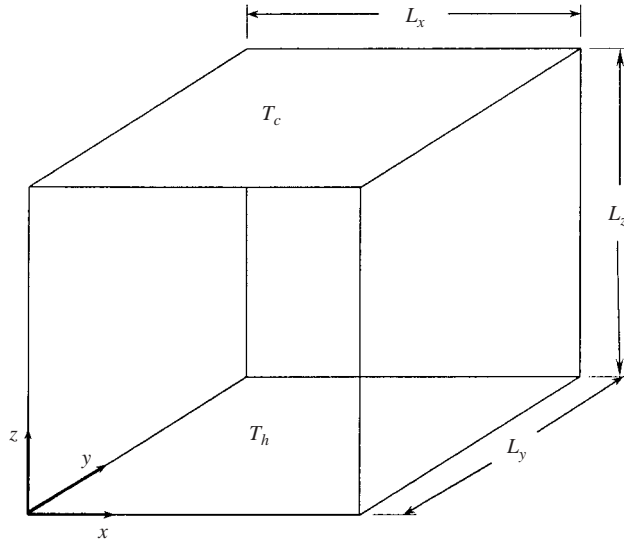


FIGURE 1. Physical model and the coordinate system.

is at a uniform, but lower, temperature  $T_c$ . The porous medium is supposed to be isotropic, homogeneous and in thermodynamic equilibrium with the fluid. All fluid properties are assumed to be constant at a reference temperature  $T_c$ , except the density in the driving term of the Navier–Stokes equations where it varies linearly with local temperature. Under these conditions the dimensionless equations governing the flow are (Nithiarasu, Seetharamu & Sundararajan 1997)

$$\nabla \cdot \mathbf{V} = 0, \tag{1}$$

$$\frac{1}{\varepsilon} \frac{\partial \mathbf{V}}{\partial t} + \frac{1}{\varepsilon^2} (\mathbf{V} \cdot \nabla) \mathbf{V} = -\nabla P + \Lambda \nabla^2 \mathbf{V} + \frac{Ra}{Pr} \theta \mathbf{k} - \frac{1}{Da} \mathbf{V} - \frac{1.75}{\sqrt{150}} \frac{|\mathbf{V}|}{\sqrt{Da}} \frac{\mathbf{V}}{\varepsilon^{3/2}}, \tag{2}$$

$$\sigma \frac{\partial \theta}{\partial t} + \mathbf{V} \cdot \nabla \theta = \frac{1}{Pr} \lambda \nabla^2 \theta, \tag{3}$$

where  $\mathbf{V}$ ,  $P$  and  $\theta$  are dimensionless velocity vector, pressure and temperature defined as  $\mathbf{V} = \mathbf{v}L_z/\nu$ ,  $P = pL_z^2/\rho\nu^2$  and  $\theta = (T - T_c)/(T_h - T_c)$  and  $\mathbf{v}$  is the velocity vector,  $\nu$  is the kinematic viscosity of the fluid,  $p$  is the pressure,  $\rho$  is the density of the fluid and  $T$  is the temperature. The length scales are non-dimensionalized by  $L_z$ . In (1)–(3),  $Ra = (g\beta(T_h - T_c))L_z^2/\nu\alpha$  is the thermal Rayleigh number,  $Da = K/L_z^2$  is the Darcy number,  $Pr = \nu/\alpha$  is the Prandtl number,  $\alpha = k/\rho C_p$  is the effective thermal diffusivity,  $k$  is the effective thermal conductivity of the porous medium,  $\varepsilon$  is the porosity and  $K$  is the permeability of the medium,  $\beta$  is the thermal expansion coefficient of the fluid,  $g$  is the acceleration due to gravity,  $C_p$  is the specific heat,  $\mathbf{k}$  is the unit vector in the vertical direction. The parameter  $\lambda = k_m/k_f$  is the ratio of thermal conductivities of the porous medium and the fluid and  $\sigma = [\varepsilon(\rho C_p)_f + (1 - \varepsilon)(\rho C_p)_s]/(\rho C_p)_f = (\rho C_p)_m/(\rho C_p)_f$  is the heat capacity ratio. The second term on the right-hand side of the momentum equation is the Brinkman term, which is included to account for the viscous stresses adjacent to the enclosure walls. The parameter  $\Lambda = \mu_e/\mu$  is the ratio of the effective viscosity in the Brinkman term to the fluid viscosity. The variation of  $\Lambda$  is not fully understood and most of the works on non-Darcy formulation take  $\Lambda = 1$ . The last term

in the momentum equations is the Forchheimer term and represents the nonlinear drag effect due to the solid matrix, where Ergun's (1952) correlation is used with the total velocity vector  $|\mathbf{V}| = (U^2 + V^2 + W^2)^{0.5}$ . Even though the contribution of the advection terms is small, they are included in the model to handle all possible situations. The inclusion of the advection terms is also necessary for smooth development of the boundary layer near the enclosing walls (Vafai & Kim 1995).

The non-dimensional boundary conditions are:

$$U = V = W = \frac{\partial \theta}{\partial X} = 0 \quad \text{for } X = 0, 1, \quad (4)$$

$$U = V = W = \frac{\partial \theta}{\partial Y} = 0 \quad \text{for } Y = 0, 1, \quad (5)$$

$$U = V = W = 0, \theta = 1, \quad \text{for } Z = 0, \quad (6)$$

$$U = V = W = 0, \theta = 0, \quad \text{for } Z = 1, \quad (7)$$

where  $U$ ,  $V$ ,  $W$  are the  $x$ ,  $y$  and  $z$  components of the velocity vector, respectively.

### 3. Method of solution

The governing equations are integrated directly in space and time and are discretized by using the finite-volume method. However, unlike direct studies of stability and multiplicity, which involve calculation of the Jacobian matrices, their determinants and eigenvalues, the unstable solutions cannot be captured with the present method. Staggered non-uniform grids are generated such that denser grid clustering is obtained near the enclosure walls. The QUICK scheme (Leonard 1979) is used to calculate the convection of a scalar term at a control volume face. A high-resolution flux limiter known as ULTRA-SHARP (Leonard & Mokhtari 1990) is used to eliminate oscillations in the high-gradient regions. The flux term is applied using a deferred correction technique to reduce the stencil of the discrete equations. In this technique, the flux value estimated by the QUICK scheme is written as the sum of the first-order upwind term plus a correction term, which provides higher accuracy. The first-order upwind term is treated implicitly, while the correction term is treated explicitly and added to the source term. The discretized mass momentum and energy equations are solved in a segregated approach using the standard SIMPLEC algorithm (Van Doormaal & Raithby 1984). The momentum equations are solved by using the iterative method SIP of Stone (1968), which is extended here to handle three-dimensional problems. Conjugate gradient (Hackbusch 1994) and Bi-CGSTAB iterative methods (Van der Vorst 1992) are used to solve the pressure correction and energy equations, respectively. Iterations are continued until the second norm of the residuals for all equations reduced below  $10^{-6}$ . No significant variations are observed at this residual level.

A full approximation storage (FAS) full multigrid (FMG) method (Hortmann, Peric & Scheurer 1990) is used to solve the problem.  $82 \times 82 \times 82$  control volumes are used on the finest level for all cases except for the time-dependent solutions where  $42 \times 42 \times 42$  control volumes are used. The time stepping has been realized with the second-order fully implicit backward Euler scheme. The time step used was between 0.01 and 0.0001, depending on the Rayleigh number used. By this means, a minimum of 50 points in a period of oscillations is ensured in order to capture the time-dependent solutions with reasonable accuracy. The maximum computer time was about two days for the highly oscillatory high-Rayleigh-number cases, where a

1.8 GHz PC was used. The computer code has been validated for various cases and the results published elsewhere (Sezai & Mohamad 1999, 2000).

#### 4. Results and discussion

Simulations were carried out starting with the diffusion solution and increasing the porous thermal Rayleigh number  $Ra^* = RaDa$  up to 1000. The results obtained from the previous run were used as initial conditions for the next run. The Prandtl number of the fluid is fixed at  $Pr = 10$ . The thermal properties of the solid porous matrix and the fluid have been taken to be identical so that  $\lambda = 1$  and  $\sigma = 1$ . The porosity of the medium is assumed to be uniform throughout the domain and to remain constant at  $\varepsilon = 0.6$ . The remaining properties of the porous medium are set as  $\Lambda = 1$  and  $Da = 10^{-5}$ .

##### 4.1. Symmetry properties

The solution of the problem has symmetries due to the invariance properties of the governing equations with the boundary conditions used. It is essential to understand the symmetries of the problem in order to classify the resulting flow patterns in terms of symmetry groups. In this section we give a brief description of the symmetry groups we shall encounter.

Rotational symmetry with respect to a vertical axis (parallel to the  $z$ -axis) at  $X = 0.5, Y = 0.5$  is denoted by  $r_z$ , which is the mapping consisting of a rotation of  $90^\circ$  about that axis. Rotational symmetry  $r_z^2$  is the mapping which consists of a rotation of  $180^\circ$  about the same axis. Here,  $r_z^2$  stands for  $r_z r_z$  which means applying symmetry  $r_z$  twice. Similarly,  $r_z^3$  corresponds to a  $270^\circ$  rotation about the vertical centreline. Rotational symmetries  $r_x$  and  $r_y$  refer to symmetries with respect to the horizontal axis parallel to the  $x$ - and  $y$ -axis, respectively. Plane symmetries are denoted by letter  $s$ . For example, plane symmetry  $s_x$  is the mapping which produces the mirror image of the flow and temperature fields about the  $X = 0.5$  plane. Similarly  $s_y, s_d, s_d'$  refer to plane symmetries about plane  $Y = 0.5$ , diagonal plane  $X = Y$  and diagonal plane  $X = -Y$ , respectively.

The mathematical descriptions of the above symmetries are given in Sezai (2002) and will not be repeated here. The simplest symmetry group is  $Z_2$  and refers to any group having a single symmetry generated by a plane reflection or  $180^\circ$  rotation. For example, the single plane reflections generate the symmetry groups,  $\{e, s_x\}, \{e, s_y\}, \{e, s_d\}, \{e, s_d'\}$ , where  $e$  is the identity. A rotation of a  $180^\circ$  about the vertical axis generates the symmetry group  $\{e, r_z^2\}$ . All these single symmetry groups are described as group  $Z_2$ . Applying the symmetry operations  $s_x$  and  $s_y$  consecutively is equivalent to a  $180^\circ$  rotation about a vertical axis, that is,  $r_z^2 = s_x s_y$ . Similarly, application of the symmetry operations  $s_x$  and  $s_d$  consecutively is equivalent to a  $90^\circ$  rotation, or  $r_z = s_x s_d$ . Applying the same plane symmetry operation twice results in the identity,  $e$  that is,  $s_x^2 = s_y^2 = e$ . A rectangle has three symmetries:  $180^\circ$  rotation  $r_z^2$ , as well as plane symmetries  $s_x$  and  $s_y$ . This symmetry group is named  $D_2$  and defined by  $\{e, s_x, s_y, r_z^2\}$ . The group  $D_2$  has three subgroups  $\{e, s_x\}, \{e, s_y\}$  and  $\{e, r_z^2\}$ . Any two of these  $Z_2$  subgroups can be combined to form  $D_2$  and is written as  $D_2 = Z_2 \times Z_2$ . A square has four more symmetries:  $s_d$  and  $s_d'$  corresponding to reflection symmetries about the two diagonals and  $r_z$  and  $r_z^3$  corresponding to  $90^\circ$  and  $270^\circ$  rotations about the vertical axis. This symmetry group is named  $D_4$  and is defined by

$$\{e, s_x, s_y, s_d, s_d', r_z, r_z^2, r_z^3\}.$$

---

Structure	Symmetry	Symmetry group
S1	$\{e, s_d\}$	$Z_2$
S2	$\{e, s_x, \tau_x\}$	$O(2)$
S3	$\{e, s_d, s_d', r_z^2\}$	$D_2$
S4	$\{e, s_x, s_y, \tau_y\}$	$Z_2 \times O_2$
S5	$\{e, s_x, s_y, s_d, s_d', r_z, r_z^2, r_z^3\}$	$D_4$
S6	None	None
S7	$\{e, s_x, s_y, r_z^2\}$	$D_2$
S8	$\{e, r_z^2\}$	$Z_2$
S9	$\{e, r_z, r_z^2, r_z^3\}$	$Z_4$
S10	$\{e, s_d\}$	$Z_2$

---

TABLE 1. Symmetries contained in the steady flow patterns.

The cyclic group  $Z_4$  has four elements,  $\{e, r_z, r_z^2, r_z^3\}$ , and is one of the subgroups of  $D_4$ . These simple groups will be used to construct the symmetry groups required to describe the convection patterns.

In the present study, a total of ten steady flow patterns have been obtained above the threshold of convection start up to  $Ra^* = 1000$ . Nine of these steady flow patterns have some symmetry while one is non-symmetric. Five of the flow patterns show transient behaviour in some range of the Rayleigh number. Figure 2 shows the steady flow patterns found in this study. Here, the projection of the flow lines on the horizontal plane at  $Z = 0.9$ , the projection of the flow lines on the mid  $(x, z)$  and mid  $(y, z)$ -planes are displayed. The projections of flow lines on a particular plane are obtained from the in-plane components of the velocity vectors on that plane. The distances between the arrows on each flow line are set to a constant value from a rake position for aesthetic reasons only. The symmetries contained in each steady flow pattern are given in table 1. The three-dimensional flow trajectories of the convective patterns are displayed in figure 3. In three-dimensional flows, the flow trajectories are not necessarily closed curves. As follows from this figure, a liquid particle can travel from one convective roll to the other.

We illustrate the symmetry groups with reference to the convective patterns displayed in figure 2. The diagonal single-roll structure S1 and structure S10 have  $\{e, s_d\}$  symmetry, so they are both in the  $Z_2$  group. The single-roll structure S2 is two-dimensional. The orientation of the roll may be along the  $x$  or  $y$  direction and both are named S2. This pattern is unchanged after reflecting in the  $x$ -direction and after translating by any amount in the same direction, yielding the symmetry group  $O(2)$  of a circle under rotations and reflections. That is, in this group the pattern is unchanged under the reflection  $s_x : (X, Y, Z, t) \rightarrow (1 - X, Y, Z, t)$  and translation  $\tau_x : (X, Y, Z, t) \rightarrow (X + \lambda_x, Y, Z, t)$ . Similarly, the pattern consisting of two rolls in S4 have  $O(2)$  symmetry about the  $y$ -axis and they are also unchanged after reflecting about the  $X = 0.5$  plane, so the symmetry group of S4 is  $Z_2 \times O(2)$ . However, it should be pointed out that the translational invariance of the two-dimensional roll structures S2 and S4 is not valid near the end faces, since the confining walls distort the flow lines near the solid boundary. Structure S3 and S7 are both in the  $D_2$  symmetry group. However, S3 have  $\{e, s_d, s_d', r_z^2\}$  symmetry while S7 have  $\{e, s_x, s_y, r_z^2\}$  symmetry. Structure S5 belong to the dihedral symmetry group  $D_4$ , while structure S8 belong to the rotational symmetry group  $\{e, r_z^2\} = Z_2$ . Structure S9 belong to the rotational symmetry group  $Z_4 = \{e, r_z, r_z^2, r_z^3\}$ , while S6 is non-symmetric.

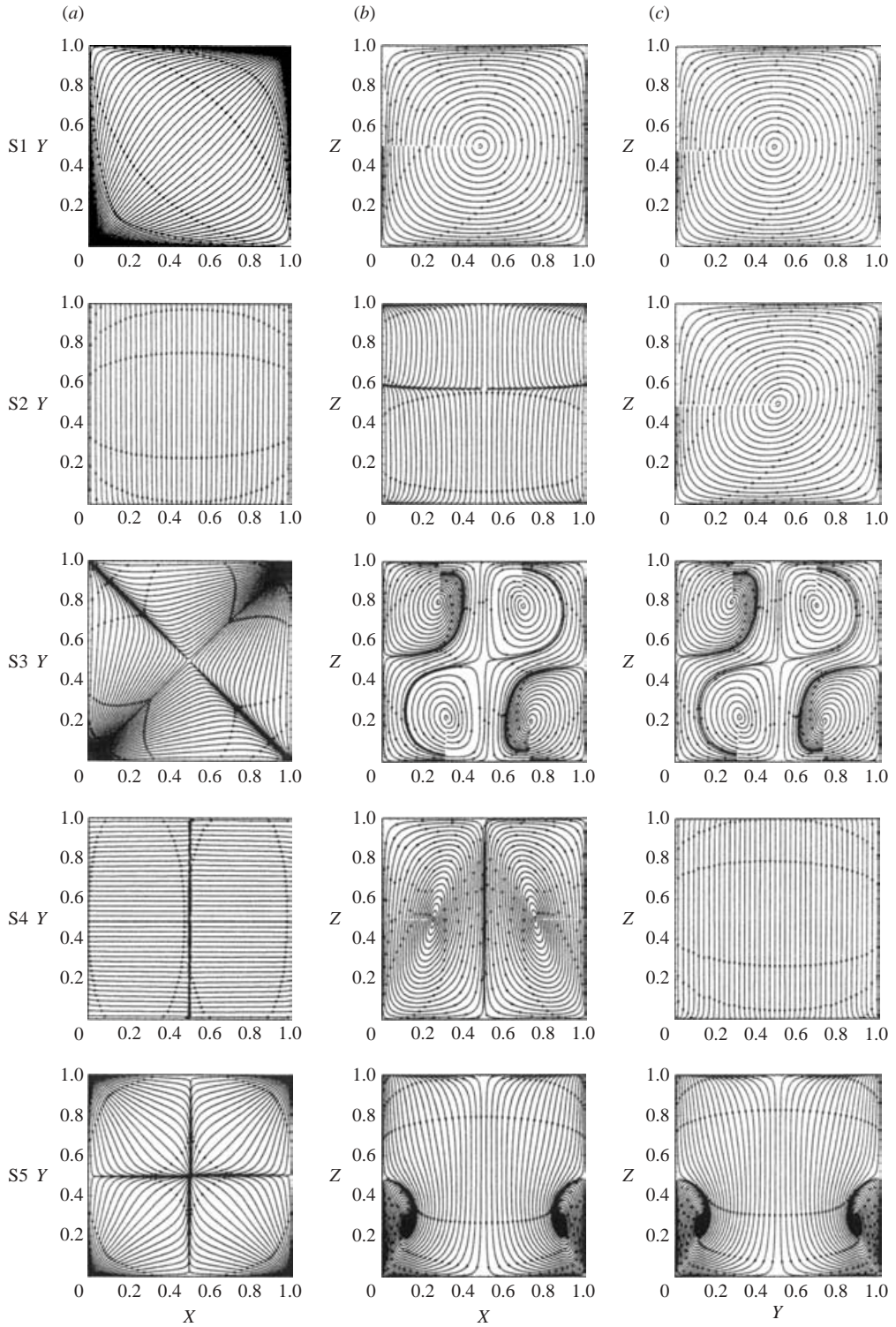


FIGURE 2. For caption see next page.

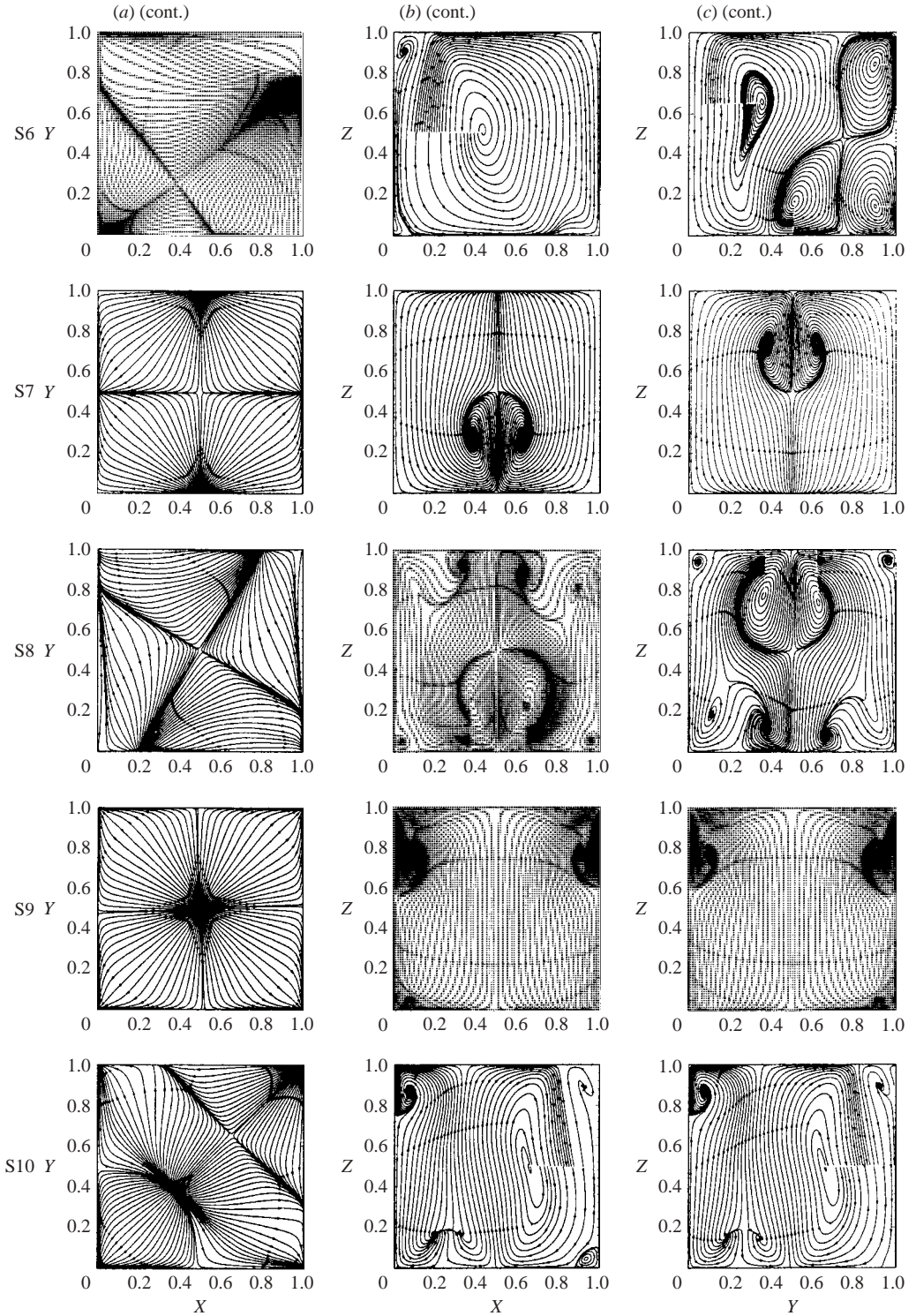


FIGURE 2. Steady-state convective patterns in the cubic cavity. (a) Projection of flow lines on the horizontal plane at  $Z = 0.9$ ; (b) projection of flow lines on the mid  $(x, z)$ -plane; (c) projection of flow lines on the mid  $(y, z)$ -plane.

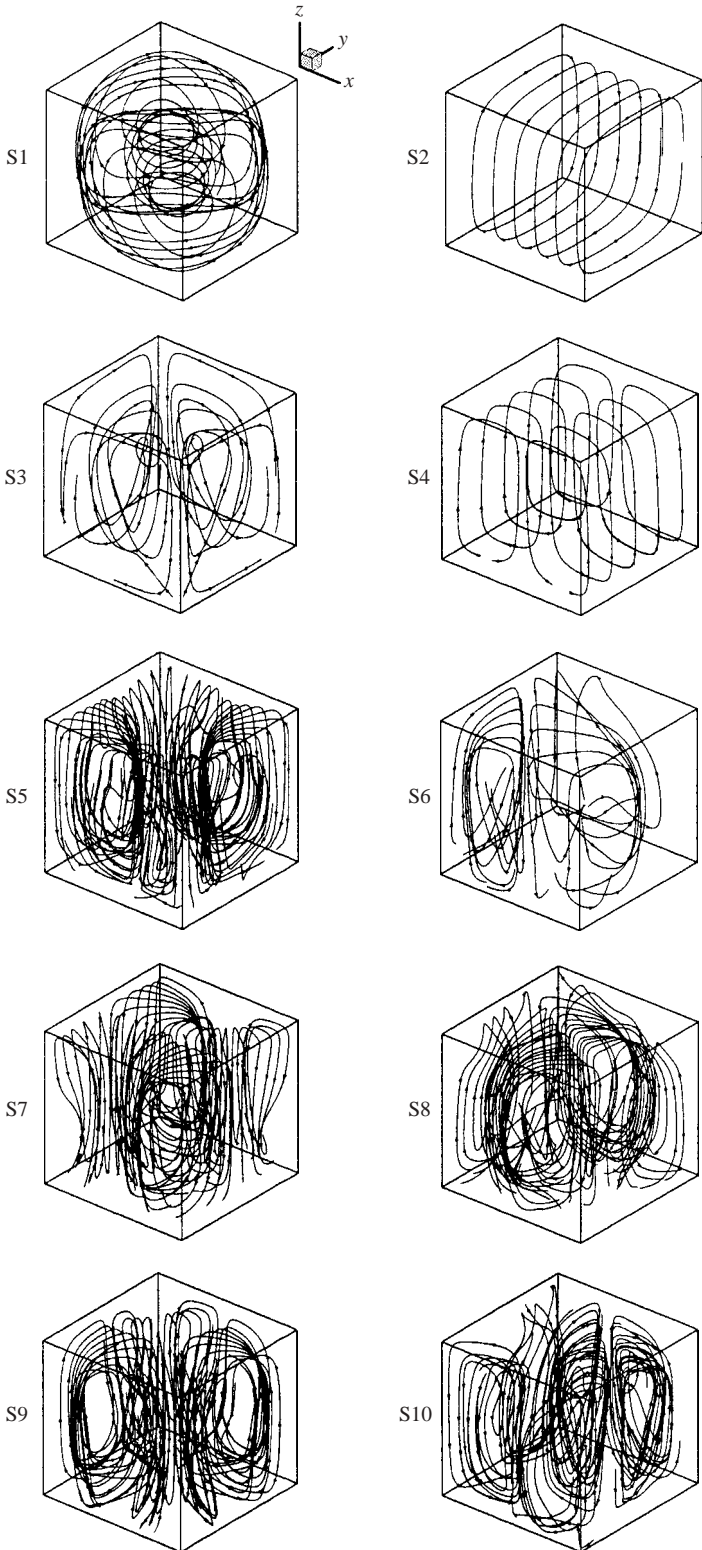


FIGURE 3. Flow trajectories of the steady convective patterns.

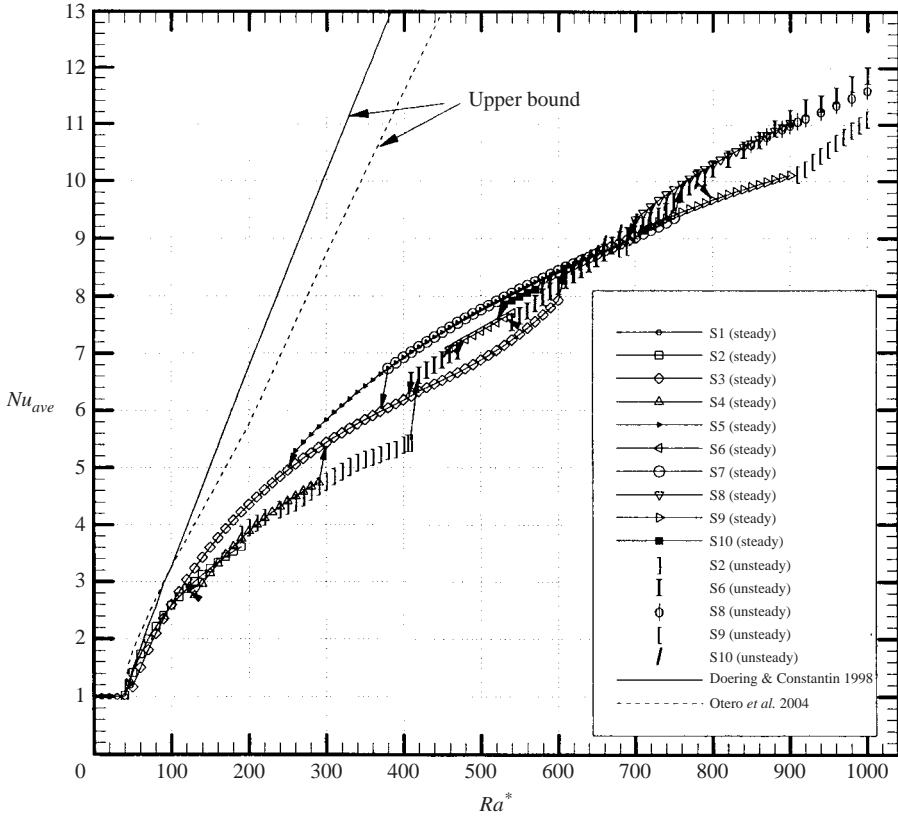


FIGURE 4. Variation of average Nusselt number with  $Ra^*$ .

4.2. Effect of Rayleigh number

Figure 4 shows the variation of the average Nusselt number of the steady and unsteady flow structures as a function of  $Ra^*$ . Unsteady convection is represented by the values of the time-averaged Nusselt number. The transitions from one flow structure to the other are shown by arrows. The transitions between the flow patterns are depicted schematically in figure 5. Included in figure 4 are the theoretical upper bounds for the Nusselt number derived by Doering & Constantin (1998) and Otero *et al.* (2004), using the infinite Prandtl–Darcy limit which provides bounds within which the predictions must lie. The upper bound is close to the numerical results near the onset of convection, but it is about a factor of three above the simulation data at the highest Rayleigh number.

The effect of the non-Darcy terms on the solution is tested by setting the Forcheimer and Brinkman terms in (2) to zero for some selected cases of structures S3 and S7. The resulting Darcy model overpredicts the flow velocities and heat transport at high Rayleigh numbers, while the results between the two models are almost the same for conditions close to the onset of convection. For example, the average Nusselt number predicted by setting non-Darcy terms to zero is 2.0% higher at  $Ra^* = 500$  and this difference increases to 6.3% at  $Ra^* = 800$ . However, the difference between the two models is not restricted to predicting different Nusselt numbers. The two models predict also a different range of existence of flow patterns and transition paths between them.

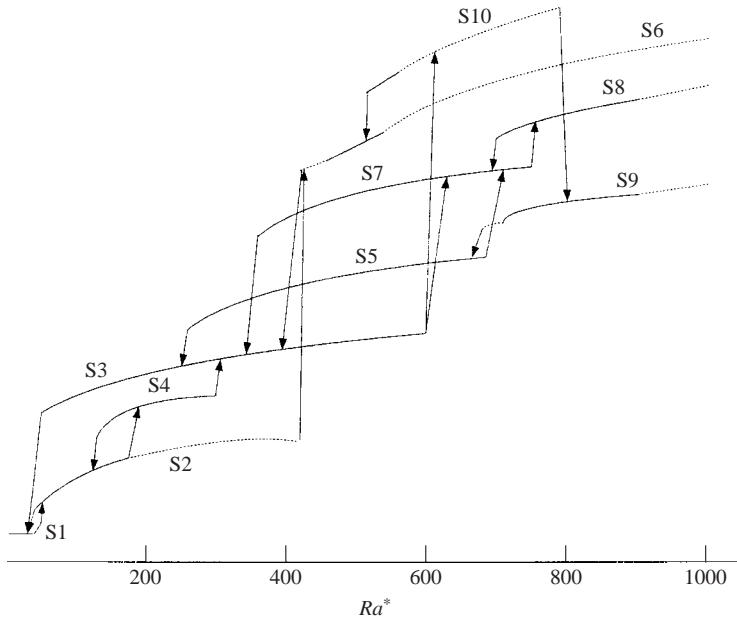


FIGURE 5. Schematic diagram of the flow transitions as a function of  $Ra^*$ . Solid (dotted) lines indicate steady (unsteady) solutions.

Starting from the motionless diffusive temperature profile as initial conditions,  $Ra^*$  is increased in steps of 10, using the results from the previous run as input for the next run. The flow structures found in the present study, their range of existence and the bifurcating solutions are summarized in table 2, together with the structures found in the previous studies. The results of the present investigation indicate that convection begins at  $Ra^* \approx 41$ , where the diffusive state undergoes a supercritical bifurcation to the two-dimensional single-roll structure S2. This value is close to the critical Rayleigh number,  $4\pi^2$ , obtained by Beck using linear stability analysis.

Another single-roll structure is S1, but unlike S2 its axis of rotation is aligned along a diagonal. Structure S1 is formed by the superposition of two horizontal orthogonal two-dimensional rolls and is stable only in a rather small range of Nusselt number, namely,  $43 \leq Ra^* \leq 46$ .

Steady, unicellular, two-dimensional convection cannot exist in a cube at porous Rayleigh numbers larger than a value somewhat below 200 (Schubert & Straus 1979). In the present study, as  $Ra^*$  is increased from 180 to 190 the steady single-cell two-dimensional convection pattern S2 undergoes a Hopf bifurcation to an oscillatory state having a single frequency. No steady two-dimensional flow pattern was found in this study for  $Ra^* > 290$ .

The flow pattern S3, which was referred to as the (1, 1, 1) mode by Straus & Schubert (1979) belongs to the symmetry group  $\{e, s_d, s_d', r_z^2\} = D_2$ . As stated earlier, Kimura *et al.* (1989) determined that the S3 mode becomes oscillatory at  $Ra^* = 575$ . In the present non-Darcy model, using no-slip boundary conditions on the enclosure walls, no oscillatory behaviour of the S3 mode was detected. Instead, the S3 mode was found to undergo a bifurcation to either S7 or S10 depending on the perturbation given by the time-step value chosen in the simulation when  $Ra^*$  is increased from 600 to 610.

Structure	Range		Structure reached upon decreasing $Ra^*$	Structure reached upon increasing $Ra^*$
	$Ra^*_{min}$	$Ra^*_{max}$		
S1 Zebib & Kassoy 1978; Horne 1979; Straus & Schubert 1981; Schubert & Straus 1979	43	46	S2	S2
S2 Holst & Aziz 1972; Zebib & Kassoy 1978; Schubert & Straus 1979; Horne 1979	41	190	Diffusive state	S2(osc.), S4
S2 (osc.)	190	410	S2	S6(osc.)
S3 Holst & Aziz 1972; Straus & Schubert 1978, 1979, 1981; Horne 1979; Steen 1983; Kimura <i>et al.</i> 1989; Stamps <i>et al.</i> 1990; Graham & Steen 1991	50	600	S2	S7, S10(osc.)
S4 Straus & Schubert 1978	130	290	S2	S3
S5	260	680	S3	S7
S6	460	540	S6(osc.)	S6(osc.)
S6(osc.)	410–420	470	S3	S6
S6*(osc.)	540–550	1000	S6	S6(osc.)
S7	380	750	S3	S8
S8	700	900	S7	S8(osc.)
S8(osc.)	850–870	1000	S8	S8(osc.)
S9	710	900	S9(osc.)	S9(osc.)
S9(osc.)	680	700	S5	S9
S9*(osc.)	910	1000	S9	S9(osc.)
S10	530	570	S6	S10(osc.)
S10(osc.)	580	780	S10	S9

TABLE 2. Flow structures, their range of existence and structures reached after bifurcation.

The bifurcation from S3 to S10 is accompanied by a loss of one of the diagonal symmetries. Upon increasing the Rayleigh number, S10 follows the route: steady  $\rightarrow$  periodic  $\rightarrow$  quasi-periodic  $\rightarrow$  chaotic until  $Ra^* = 780$ , where it bifurcates to the steady-flow structure S9 having  $Z_4 = \{e, r_z, r_z^2, r_z^3\}$  symmetry. At the lower end of the branch, structure S9 bifurcates to the steady-flow structure S5 having  $D_4$  symmetry. When  $Ra^*$  is increased from 680 to 690, the steady flow structure S5 undergoes a pitchfork bifurcation to another steady structure S7 with symmetry  $\{e, s_x, s_y, r_z^2\}$ , where the diagonal symmetries are lost. It should be noted that the average  $Nu$  values of S5 and S7 are equal for all Rayleigh numbers (figure 4). Both structures bifurcate to S3 upon decreasing  $Ra^*$  to low values. The similarities between S5 and S7 are depicted in figure 6. The rectangular box in figure 6 consists of two cubes with horizontal cross-sections  $JKFE$  and  $EFGH$ , each containing the flow structure S7. However, the pattern bounded by  $ABCD$  is recognized to be S5. Since each half of S5 is also shared by S7, then tiling of the flow pattern in S5 is lagging that of S7 by a half width. As a result they have the same Nusselt number as observed in figure 4, but have a different range of stabilities (table 2).

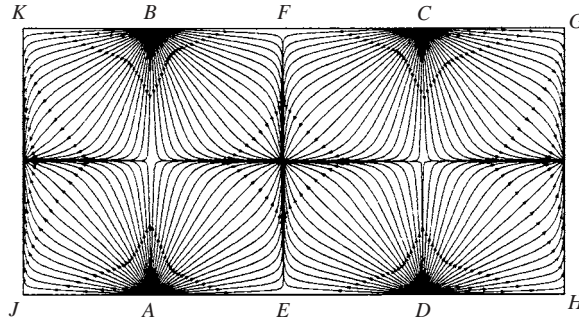


FIGURE 6. Projection of flow lines on the horizontal plane at  $Z = 0.9$  in a rectangular prism constructed from two adjacent cubes.

Broken symmetries	Resulting symmetry	Resulting pattern
None	$\{e, s_x, s_y, s_d, s_{d'}, r_z, r_z^2, r_z^3\}$	S5
$s_x, s_y, s_d, s_{d'}$	$\{e, r_z, r_z^2, r_z^3\}$	S9
$s_x, s_y, r_z, r_z^3$	$\{e, s_d, s_{d'}, r_z^2\}$	S3
$s_d, s_{d'}, r_z, r_z^3$	$\{e, s_x, s_y, r_z^2\}$	S7
$s_y, s_d, s_{d'}, r_z, r_z^2, r_z^3$	$\{e, s_x\}$	Not found
$s_y, s_d, s_{d'}, r_z, r_z^2, r_z^3$	$\{e, s_y\}$	Not found
$s_x, s_y, s_{d'}, r_z, r_z^2, r_z^3$	$\{e, s_d\}$	S1, S10
$s_x, s_y, s_d, r_z, r_z^2, r_z^3$	$\{e, s_{d'}\}$	S1, S10

TABLE 3. Possible bifurcations from  $D_4$ -symmetric flow structure S5.

The possible patterns that can generically arise through bifurcations from the four-roll structure S5, whose symmetry group is  $D_4$  or  $\{e, s_x, s_y, s_d, s_{d'}, r_z, r_z^2, r_z^3\}$ , are shown in table 3. The patterns having symmetry  $\{e, s_d\}$  or  $\{e, s_{d'}\}$  are considered to be the same in this work, as one is a  $90^\circ$ -rotated version of the other and is assigned a single name (e.g. S10). The patterns  $\{e, s_x\}$ ,  $\{e, s_y\}$ ,  $\{e, s_d\}$  and  $\{e, s_{d'}\}$  can also be reached after pitchfork bifurcations from solutions with  $D_2$  symmetry. In the present study, only S7 and S3 have been obtained through bifurcations directly from S5. All other three-dimensional patterns were obtained through bifurcations from  $D_2$ -symmetric solutions (S3 and S7), which originated from the  $D_4$  solution. No two-dimensional flow patterns were obtained through bifurcations from three-dimensional patterns. In the study of Rucklidge *et al.* (2000), it has been shown that not all subgroups of  $D_4$  are possible symmetry groups of bifurcating solutions: in particular,  $\{e, r_z^2\}$  is not an isotropy subgroup of any bifurcating solution. It can only appear after two successive bifurcations from  $D_4$  symmetry. This is verified in the present study. For example, the structure S8 with  $\{e, r_z^2\}$  symmetry was obtained after two successive bifurcations from the  $D_4$ -symmetric solution S5; first to  $D_2$ -symmetric structure S7 then from S7 to S8. Similarly, solutions lacking all symmetry are only attainable after several bifurcations. For example, the non-symmetric flow structure S6 evolves after the bifurcation sequence S5 ( $D_4$  symmetry)  $\rightarrow$  S3 ( $D_2$  symmetry)  $\rightarrow$  S10 ( $Z_2$  symmetry)  $\rightarrow$  S6 (non-symmetric). Although the flow patterns with  $\{e, s_x\}$  and  $\{e, s_y\}$  symmetry are possible subgroups of  $D_4$ -symmetric structure S5, no flow patterns with either symmetry were obtained in this study.

The symmetries of the solution, which are due to the invariance properties of the governing equations and the boundary conditions, are always restricted by the symmetries of the bounding geometry. For example, in a cavity of a square horizontal cross-section, heated from below and cooled from the top, the flow pattern with the maximum number of symmetries will have all the symmetries of a square, or the symmetries  $D_4 = \{e, s_x, s_y, s_d, s_d', r_z, r_z^2, r_z^3\}$ . This structure is S5. Similarly, in a cavity of a rectangular horizontal cross-section, the flow pattern, at most, can have symmetries  $D_2 = \{e, s_x, s_y, r_z^2\}$  or the symmetries of a rectangle. This type of a flow pattern will result if S5 is used as the initial profile and the  $x$ - $y$  square cross-section of the cube is changed into a rectangle by increasing  $L_x$ , while keeping  $L_y$  and  $L_z$  constant. In that case, the flow pattern will be a deformed S5 in order to conform to the bounding geometry. Then, the possible patterns that can generically arise in a rectangular prism through bifurcations from the deformed form of S5, whose symmetry group is  $D_2$  or  $\{e, s_x, s_y, r_z^2\}$  are  $\{e, r_z^2\}$ ,  $\{e, s_x\}$  and  $\{e, s_y\}$ .

Bifurcations from an oscillatory state to another oscillatory structure are also possible. For example, single-roll two-dimensional structure S2 follows the route: steady  $\rightarrow$  periodic  $\rightarrow$  quasi-periodic  $\rightarrow$  periodic and then bifurcates to the periodic state of the non-symmetric structure S6. No steady-flow structures could be obtained for  $Ra^* > 900$ , where only S8 and S9 are found to reach this limit. In all previous studies, the maximum Rayleigh number for steady-flow solutions in a cube have been reported to be much lower. For example, Kimura *et al.* (1989) set the maximum value of  $Ra^*$  to be around 575 before oscillations begin. However, the flow pattern they studied was S3 of which no oscillatory branch could be found in the present study.

Figure 7 displays the distribution of Nusselt number on the top and bottom walls of the cubic cavity. In these plots, a maximum value of the Nusselt number corresponds to a region of impingement of an ascending flow on the top plate or descending flow on the bottom plate. Relatively low values of  $Nu$  correspond to stagnant regions of boundary-layer flow for the fluid leaving the surface. Structures S3, S6, S7 and S8 have a common feature in that all have two counter-rotating rolls of which the axis of rotation is not stationary, but rotates  $90^\circ$  in the horizontal plane as the fluid ascends from bottom to top. This is reflected in the Nusselt-number distribution where the line along which  $Nu$  is a minimum on the bottom plate, is rotated  $90^\circ$  on the top plate.

## 5. Conclusions

In this paper, the evolution of the convection patterns in a fluid-saturated porous cube heated from below is studied as a function of the Rayleigh number. The present model uses a non-Darcy model and no-slip boundary conditions for velocities at the rigid boundaries.

At low  $Ra^*$  values, the results of the present model generally agree with previous results found under the assumption of the Darcy law and zero shear stress at the solid boundaries. However, for  $Ra^* > 130$ , new flow patterns have been found to exist in addition to those mentioned in the previous studies. No steady two-dimensional flow pattern was found in this study for  $Ra^* > 290$ . In the present study, a total of ten steady flow patterns have been identified, of which five show oscillatory behaviour in some Rayleigh-number range. However, the oscillatory convection of only pattern S3 has been identified in all previous studies of three-dimensional convection in a porous cube. In the present study, the S3 mode shows no oscillatory behaviour.

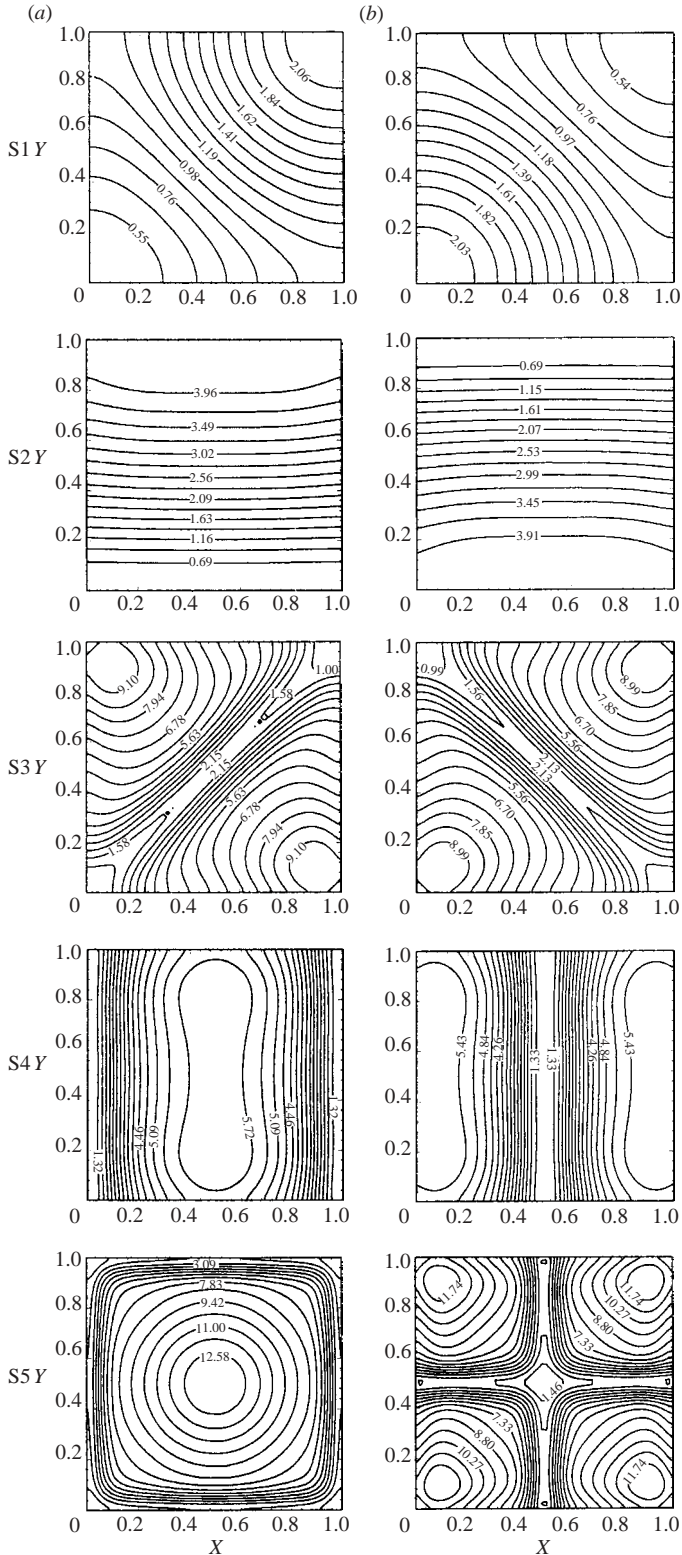


FIGURE 7. For caption see next page.

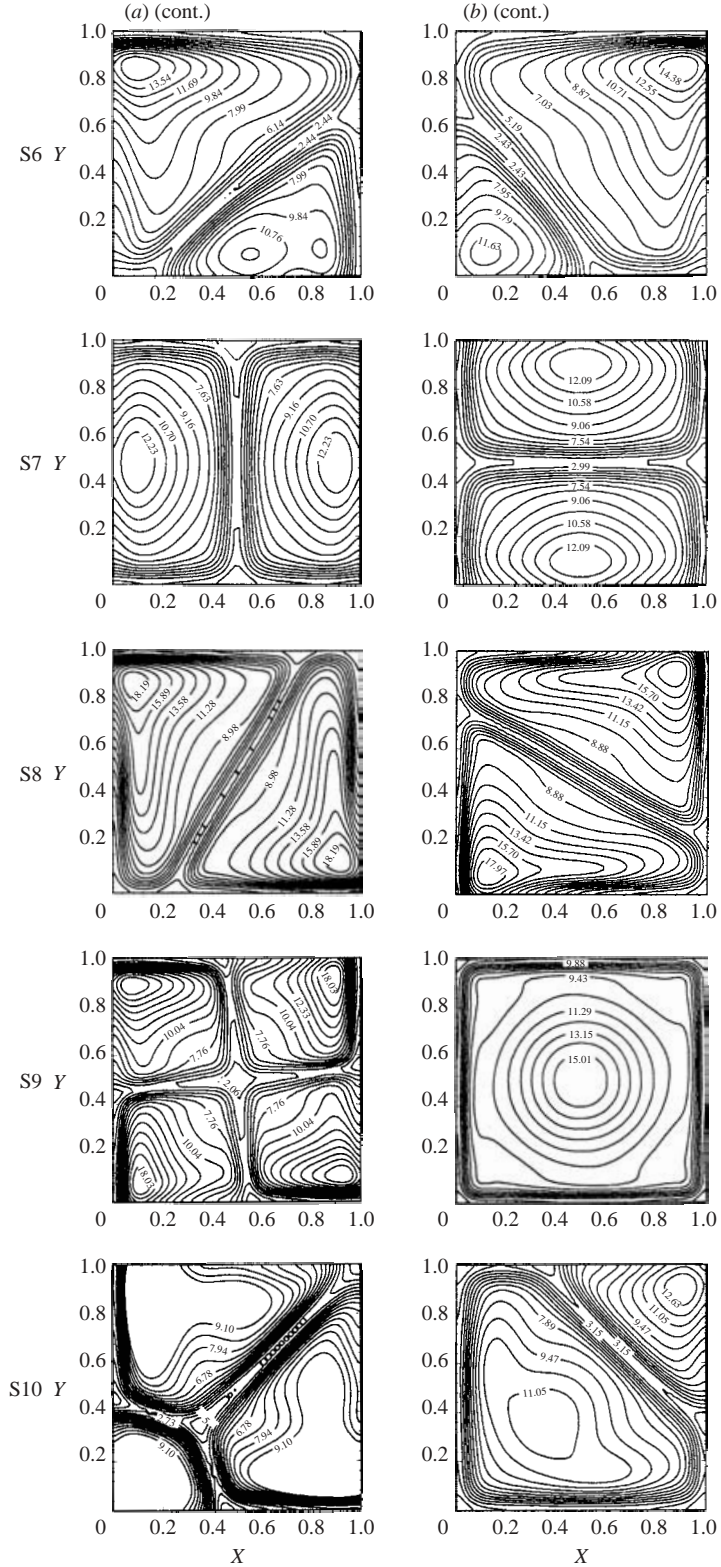


FIGURE 7. The distribution of the Nusselt number on (a) the top and (b) the bottom walls of the cubic cavity.

The steady-flow structure S3 is stable in a rather wide range of Rayleigh number ( $50 \geq Ra^* \geq 600$ ). All other structures have a narrower range of stabilities.

Not all of the unsteady modes can exist at the highest Rayleigh number ( $Ra^* = 1000$ ) investigated. The oscillatory mode of the two-dimensional single-roll structure S2 cannot exist for Rayleigh numbers greater than 400, where it bifurcates to the oscillatory mode of the non-symmetric flow structure S6. Similarly, the oscillatory mode of the  $Z_2$ -symmetric flow structure S10, with symmetry  $\{e, s_d\}$ , can exist only up to  $Ra^* = 780$ , where it bifurcates to the steady,  $Z_4$ -symmetric structure S9.

From the possible patterns that can generically arise through bifurcations from the four-roll structure S5, whose symmetry group is  $D_4$ , all flow patterns except the one with either  $\{e, s_x\}$  or  $\{e, s_y\}$  symmetry have been obtained in this study. Of these possible bifurcating solutions, only S7 and S3 have been obtained through bifurcations directly from S5. All other possible patterns were obtained through pitchfork bifurcations from  $D_2$  symmetric solutions (S3 and S7), which originated from the  $D_4$  solution. Structure S8 with  $\{e, r_z^2\}$  symmetry was obtained after two successive bifurcations from  $D_4$  symmetric solution S5; first to  $D_2$  symmetric structure S7 then from S7 to S8. A similar observation was made by Rucklidge *et al.* (2000) for magneto-convection in a square box with periodic lateral boundary conditions that  $\{e, r_z^2\}$  is not an isotropy subgroup of any bifurcating solution from  $D_4$  symmetry and that it can only appear after two successive bifurcations from  $D_4$  symmetry.

Although the flow patterns with  $\{e, s_x\}$  and  $\{e, s_y\}$  symmetry are possible subgroups of  $D_4$ -symmetric structure S5, no flow patterns with either symmetry was obtained in this study.

Also, no two-dimensional flow patterns were obtained through bifurcations from three-dimensional patterns.

The maximum Rayleigh number for obtaining steady solutions is found to be 900, where only S8 and S9 are found to reach this limit. In all previous studies, the maximum Rayleigh number for steady-flow solutions in a cube have been reported to be much lower. For example, Kimura *et al.* (1989) set the maximum value of  $Ra^*$  to be around 575 before oscillations begin. However, they used stress-free boundary conditions at rigid walls and the flow pattern they studied was S3, of which no oscillatory branch could be found in the present study.

#### REFERENCES

- BECK, J. L. 1972 Convection in a box of porous material saturated with fluid. *Phys. Fluids* **15**, 1377–1383.
- CALTAGIRONE, J. P. 1975 Thermoconvective instabilities in a horizontal porous layer. *J. Fluid Mech.* **72**, 269–287.
- DOERING, C. R. & CONSTANTIN, P. 1998 Bounds for heat transport in a porous layer. *J. Fluid Mech.* **376**, 263–296.
- ERGUN, S. 1952 Fluid flow through packed column. *Chem. Engng Prog.* **48**, 89–94.
- GRAHAM, M. D. & STEEN, P. H. 1991 Structure and mechanism of oscillatory convection in a cube of fluid saturated porous material heated from below. *J. Fluid Mech.* **232**, 591–609.
- GRAHAM, M. D. & STEEN, P. H. 1994 Plume formation and resonant bifurcations in porous media convection. *J. Fluid Mech.* **272**, 67–89.
- HACKBUSCH, W. 1994 *Iterative Solution of Large Sparse Systems of Equations*. Springer.
- HOLST, P. H. & AZIZ, K. 1972 Transient three-dimensional natural convection in confined porous media. *J. Fluid Mech.* **15**, 73–90.
- HORNE, R. N. 1979 Three-dimensional natural convection in a confined porous medium heated from below. *J. Fluid Mech.* **92**, 751–766.

- HORNE, R. N. & O'SULLIVAN, M. J. 1974 Oscillatory convection in a porous medium heated from below. *J. Fluid Mech.* **66**, 339–352.
- HORTMANN, M., PERIC, M. & SCHEUERER, G. 1990 Finite volume multigrid prediction of laminar natural convection: bench-mark solutions. *Intl J. Numer. Meth. Fluids* **11**, 189–207.
- KIMURA, S., SCHUBERT, G. & STRAUS, J. M. 1987 Instabilities of steady, periodic and quasi-periodic modes of convection in porous media. *J. Heat Transfer* **109**, 350–355.
- KIMURA, S., SCHUBERT, G. & STRAUS, J. M. 1989 Time-dependent convection in a fluid saturated porous cube heated from below. *J. Fluid Mech.* **207**, 153–189.
- LAPWOOD, E. R. 1948 Convection of a fluid in a porous medium. *Proc. Camb. Phil. Soc.* **44**, 508–521.
- LEONARD, B. P. & MOKHTARI, S. 1990 Beyond first order upwinding: the ULTRA-SHARP alternative for nonoscillatory steady-state simulation of convection. *Intl J. Numer. Meth. Engng* **30**, 729–766.
- LEONARD, P. 1979 A stable and accurate convective modeling procedure based on quadratic upstream interpolation. *Comput. Meth. Appl. Mech. Engng* **19**, 59–98.
- NITHARASU, P., SEETHARAMU, K. N. & SUNDARARAJAN, T. 1997 Natural convective heat transfer in a fluid saturated variable porosity medium. *Intl J. Heat Mass Transfer* **40**, 3955–3967.
- OTERO, J., DONTCHEVA, L. A., JOHNSTON, H., WORTHING, R. A., KURGANOV, A., PETROVA, G. & DOERING, C. R. 2004 High-Rayleigh number convection in a fluid-saturated porous layer. *J. Fluid Mech.* **500**, 263–281.
- RILEY, D. S. & WINTERS, K. H. 1991 Time periodic convection in porous media: the evolution of Hopf bifurcations with aspect ratio. *J. Fluid Mech.* **223**, 457–474.
- RUCKLIDGE, A. M., WEISS, N. O., BROWNJOHN, D. P., MATHEWS, P. C. & PROCTOR, M. R. E. 2000 Compressible magnetoconvection in three-dimensions: pattern formation in a strongly stratified layer. *J. Fluid Mech.* **419**, 283–323.
- SCHUBERT, G. & STRAUS, J. M. 1979 Three-dimensional and multicellular steady and unsteady convection in fluid-saturated porous media at high Rayleigh numbers. *J. Fluid Mech.* **94**, 25–38.
- SCHUBERT, G. & STRAUS, J. M. 1982 Transitions in time dependent thermal convection in fluid saturated porous media. *J. Fluid Mech.* **121**, 301–313.
- SEZAI, I. 2002 Flow transitions in three-dimensional double-diffusive fingering convection in a porous cavity. *J. Fluid Mech.* **464**, 311–344.
- SEZAI, I. & MOHAMAD, A. A. 1999 Three-dimensional double-diffusive convection in a porous cubic enclosure due to opposing gradients of temperature and concentration. *J. Fluid Mech.* **400**, 333–353.
- SEZAI, I. & MOHAMAD, A. A. 2000 Natural convection in a rectangular cavity heated from below and cooled from top as well as the sides. *Phys. Fluids* **12**, 432–443.
- STAMPS, D. W., ARPACI, V. S. & CLARK, J. A. 1990 Unsteady three-dimensional natural convection in a fluid-saturated porous medium. *J. Fluid Mech.* **213**, 377–396.
- STEEN, P. H. 1983 Pattern selection for finite-amplitude convection states in boxes of porous media. *J. Fluid Mech.* **136**, 219–241.
- STONE, H. L. 1968 Iterative solution of implicit approximations of multi-dimensional partial differential equations. *SIAM J. Numer. Anal.* **5**, 530–558.
- STRAUS, J. M. 1974 Large amplitude convection in porous media. *J. Fluid Mech.* **64**, 51–63.
- STRAUS, J. M. & SCHUBERT, G. 1978 On the existence of three-dimensional convection in a rectangular box containing fluid-saturated porous material. *J. Fluid Mech.* **87**, 385–394.
- STRAUS, J. M. & SCHUBERT, G. 1979 Three-dimensional convection in a cubic box of fluid saturated porous material. *J. Fluid Mech.* **91**, 155–165.
- STRAUS, J. M. & SCHUBERT, G. 1981 Modes of finite amplitude three-dimensional convection in rectangular boxes of fluid-saturated porous material. *J. Fluid Mech.* **103**, 23–32.
- VAFAI, K. & KIM, S. J. 1995 On the limitations of the Brinkman–Forchheimer-extended Darcy equation. *Intl J. Heat Fluid Flow* **16**, 11–15.
- VAN DER VORST, H. A. V. 1992 BICGSTAB: a fast and smoothly converging variant of Bi-CG for the solution of non-symmetric linear systems. *SIAM J. Sci. Statist. Comput.* **13**, 631–644.
- VAN DOORMAAL J. P. & RAITHYBY G. D. 1984 Enhancements of the SIMPLE method for predicting incompressible fluid flows. *Numer. Heat Transfer* **7**, 147–163.
- ZEBIB, A. & KASSOY, D. R. 1978. Three-dimensional natural convection motion in a confined porous medium. *Phys. Fluids* **21**, 1–3.